IOPscience iopscience.iop.org

Home Search Collections Journals About Contact us My IOPscience

Paraconductivity of oxygen-deficient $YBa_2Cu_3O_x$ thin films

This article has been downloaded from IOPscience. Please scroll down to see the full text article.

2001 J. Phys.: Condens. Matter 13 875

(http://iopscience.iop.org/0953-8984/13/5/308)

View the table of contents for this issue, or go to the journal homepage for more

Download details:
IP Address: 171.66.16.226
The article was downloaded on 16/05/2010 at 08:26

Please note that terms and conditions apply.

INSTITUTE OF PHYSICS PUBLISHING JOURNAL OF PHYSICS: CONDENSED MATTER

J. Phys.: Condens. Matter **13** (2001) 875–888 www.iop.org/Journals/cm PII: S0953-8984(01)18122-1

Paraconductivity of oxygen-deficient $YBa_2Cu_3O_x$ thin films

A Gueffaf, M Salim and M S Raven

School of Electrical and Electronic Engineering, University of Nottingham, Nottingham NG7 2RD, UK

Received 19 October 2000, in final form 29 November 2000

Abstract

The paraconductivity of a number of *c*-axis-oriented $YBa_2Cu_3O_x$ thin films, with a range of *c*-axis lattice parameters and T_c-values, has been determined as a function of temperature and analysed in terms of the paraconductivity due to direct and indirect fluctuation contributions. We present results on the *c*-axis coherence length and the phase-relaxation time at 100 K obtained from the fit to the paraconductivity data. The paraconductivity results for optimally doped films were: *c*-axis coherence length: $\xi_c(0) = 1.25$ Å; pair-breaking parameter: $\delta = 0.05$; phase-relaxation time at 100 K: $\tau_\phi = 0.066$ ps; and two–three-dimensional crossover temperature: $T^+ = 96.6$ K. These values are in good agreement with those from other published work. There was considerable scatter in the coherence length and phase-relaxation time for films with different critical temperatures and oxygen contents. These results were process dependent but appear to be related to the 60 K phase transition in the T_c–x phase diagram.

1. Introduction

One of the most common observations related to the occurrence of superconductivity is the sharp decrease in resistivity at the critical temperature T_c. The fact that the change in resistivity is not perfectly abrupt has been of interest for many years. Apart from the finite transition width caused by the sensitivity and resolution of the measuring technique (extrinsic broadening), the transition width broadening caused by *intrinsic* material properties can provide insight into the fundamental mechanism of superconductivity. Thus as the material temperature decreases towards T_c, fluctuating pairs begin to be created spontaneously. As the temperature approaches T_c, the number of pairs increases rapidly at the expense of the normal electron density. The normal-state resistance decreases and the net resistance decreases due to short-circuiting by the superfluid, a process referred to as *paraconductivity* [1–4]. In high-temperature superconductors, critical temperatures can be higher than 100 K, so a few superconducting particles may occur at significantly higher temperatures due to thermal fluctuations. Hence, the study of superconducting fluctuations is expected to be helpful in developing higher-temperature superconductors. In this case superconducting fluctuations are

0953-8984/01/050875+14$30.00 © 2001 IOP Publishing Ltd Printed in the UK

particularly significant because of the relatively high temperatures involved and coherence lengths of fractions of a nanometre. Paraconductivity measurements are therefore sensitive to material properties at the unit-cell level and have been used to yield microscopic parameters for thin films [5–13], single crystals [14–21], polycrystalline YBCO [22, 23], other cuprates [24–30] and YBCO superlattices [31]. Although this represents a fairly large body of work, there have been few systematic investigations of the paraconductivity of as-grown oxygen-deficient high-temperature superconductors.

In this paper we present paraconductivity results for a number of as-grown oxygen-deficient c-axis-oriented YBCO thin films with T_c^{mf}-values ranging from 56.6 to 92 K. By 'as-grown' we refer to the process whereby films are oxidized *in situ* during growth in the deposition system. This process is distinct from *ex situ* oxidation, whereby films are oxidized in a separate and external diffusion process. The two processes are expected to lead to different defect states [32]. In the following, we compare our experimental results with fluctuation conductivity (FC) theories. One of the significant difficulties in the measurement of paraconductivity is that of how to separate the fluctuation part from the normal-state properties. In this paper normal-state resistivity near the transition region was estimated experimentally by extrapolating the normal-state resistance from temperatures much higher than T_c, where superconducting fluctuations vanish, to temperatures below T_c [6, 33–36]. An alternative method extrapolates from an empirical equation, which fits the normal-state resistivity [14, 32, 37, 38]. From these results we determined the paraconductivity and obtained the c-axis coherence length $\xi_c(0)$, the crossover temperature T^+, the pair-breaking parameter δ and the phase-relaxation time τ_ϕ at 100 K. These values are then compared with theoretical values and values reported in the literature.

2. Experimental techniques

The YBCO thin films were grown by *in situ* off-axis r.f. magnetron sputter deposition using a stoichiometric single target and single-crystal (100)-oriented substrates [39]. These were mainly 10 mm square, 1 mm thick optically polished single-crystal (100)-oriented MgO substrates. Films were also deposited on $LaAlO_3$ and $SrTiO_3$ substrates, also (100) oriented. Prior to deposition, the substrates received a standard solvent cleaning and were finally rinsed in distilled water before being mounted on a stainless steel substrate heater. The substrates were bonded to the heater using silver foil or silver paint. Substrate temperatures were measured using a chromel/alumel (type-K) thermocouple, spot welded to the heater plate adjacent to the substrates. This temperature measurement was checked in a separate experiment by bonding a second thermocouple to the substrate surface. This indicated a temperature about 10 °C lower than that recorded by the thermocouple next to the substrate. The sputtering system had a base pressure of less than 2×10^{-6} Torr and deposition was carried out with Ar/O_2 4:1, total pressure 280 mTorr (20% or 56 mTorr of oxygen), substrate temperature between 690 and 735 °C and typical growth rates of 0.4 nm min^{-1}. At the end of the deposition period, the argon gas was turned off and the oxygen pressure increased to between 200 and 300 Torr. The substrate temperature was then decreased to 400–500 °C and the film annealed in oxygen for one hour, after which the heater was switched off and the film allowed to cool to room temperature. This procedure led to oxygen-deficient films as grown, without the need to carry out separate oxygenation and annealing experiments.

The films were analysed by means of x-ray diffraction; the results showed that the films were c-axis oriented. A typical XRD trace for YBCO sputtered on $LaAlO_3$(100) is shown in figure 1. The large number of (00l) reflections allowed measurements of the c-axis lattice parameter to within an error of less than 0.01 Å, sufficiently small for detecting changes in c due

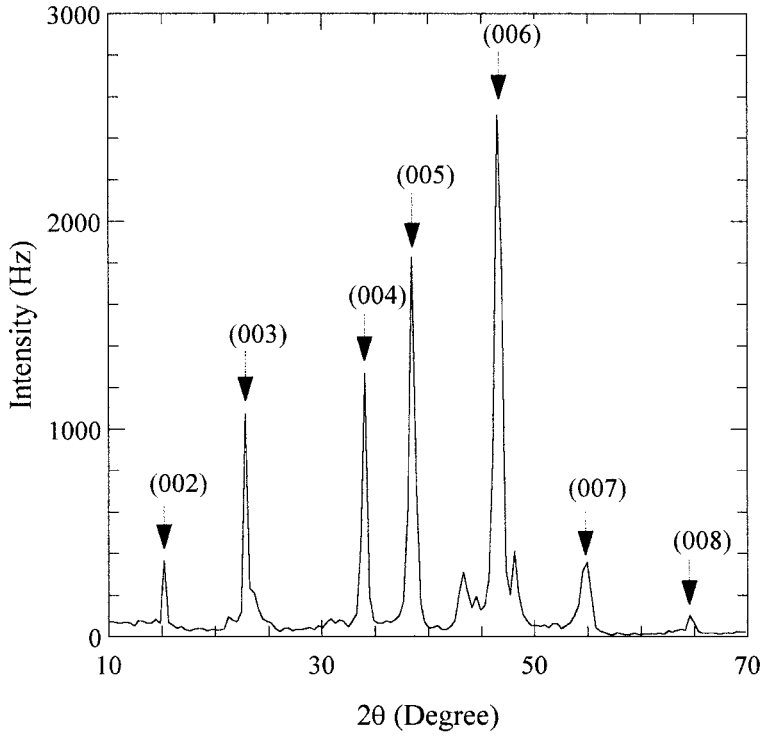

Figure 1. A typical x-ray diffraction pattern of $YBa_2Cu_3O_x$ r.f. sputtered on $LaAlO_3(100)$ showing c-axis alignment (sample Y129L).

to oxygen deficiency [40]. The oxygen content x was estimated from these lattice parameters using $x = (12.771 - c)/0.1557$, where the values are in Å units [41, 42]. The film resistivity was determined using standard four-terminal techniques. Silver pads were evaporated onto the film surface and fine copper wires bonded to four terminal pads with silver paste. Some films were patterned for Hall-effect measurements as indicated by 'P' in table 1. The samples were mounted in a temperature-controlled, closed-cycle He cryostat. The sample temperature was measured using a calibrated silicon diode sensor mounted next to the sample and connected

Table 1. The c-axis lattice parameter c, oxygen content x, mean-field critical temperature T_c^{mf}, resistivity at 300 K ρ_{300} and fitting coefficients A and B. Sample substrates: L: $LaAlO_3$; M: MgO; S: $SrTiO_3$, all (100) oriented.

Sample	c (Å)	x	T_c^{mf} (K)	ρ_{300} (mΩ cm)	A ($\mu\Omega$ cm K^{-1})	B (mΩ cm K)
1: Y123L	11.681	7.00	92	0.267	0.876	0.326
2: Y116SP	11.700	6.88	88	0.394	1.23	4.46
3: Y67M	11.715	6.78	84	0.912	2.76	34.4
4: Y129L	11.717	6.77	86	2.959	9.11	97.1
5: Y84MP	11.712	6.80	81.5	0.533	1.70	5.27
6: Y111MP	11.720	6.75	82	0.258	0.822	3.23
7: Y113MP	11.720	6.75	83	0.260	0.826	2.29
8: Y129M	11.720	6.75	81.5	1.750	5.27	65.5
9: Y78MP	11.750	6.56	56.6	1.17	3.73	28.2

to a Lakeshore temperature controller. The resistivity and temperature measurements were connected to a computer via an IEEE-488 interface bus for data collection and analysis.

3. Experimental results

The normalized resistivity, $\rho_n = \rho(T)/\rho_{300}$, versus temperature for samples with varying T_c is shown in figure 2. The resistivity values at 300 K are given in table 1. The paraconductivity, $\Delta\sigma_{xx}(T)$, was calculated by subtracting the background normal-state conductivity $\sigma_{xx}^N(T)$ from the measured conductivity:

$$\Delta\sigma_{xx}(T) = \sigma_{xx}(T) - \sigma_{xx}^N(T). \tag{1}$$

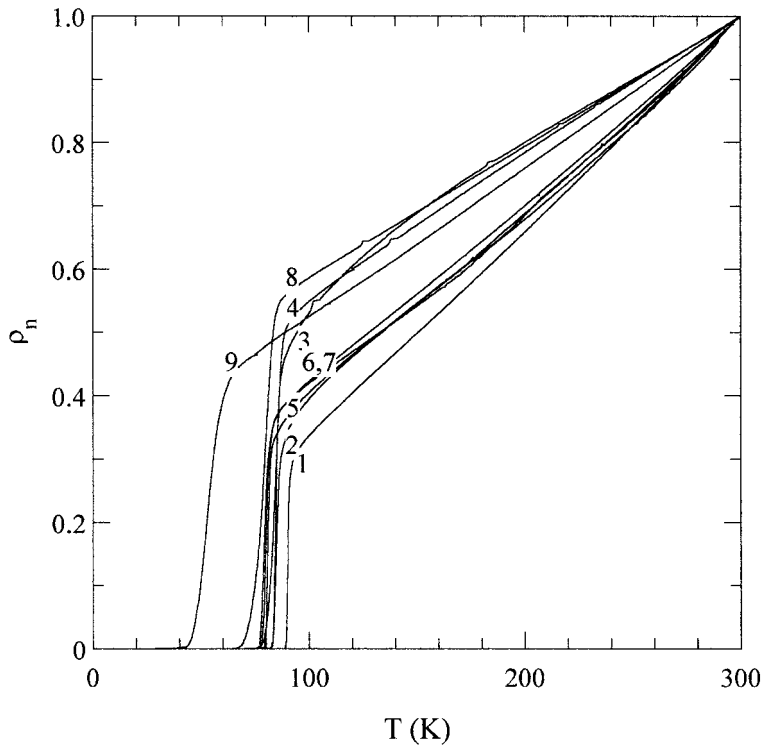

Figure 2. Normalized resistivity, $\rho_n = \rho(T)/\rho_{300}$, as a function of temperature for c-axis-oriented $YBa_2Cu_3O_x$ films with varying T_c-values. The numbers on the curves correspond to the samples listed in tables 1 and 2.

Experimentally, we measured the longitudinal resistance $R_x = V_x/I_x$ and calculated the resistivity $\rho_{xx} = wt_f R_x/l$ (with w the width, t_f the film thickness and l the distance between the voltage contacts). For orthorhombic crystals such as YBCO, $\sigma_{xx} = 1/\rho_{xx}$. Hence the excess conductivity is

$$\Delta\sigma_{xx}(T) = \frac{\rho_{xx}^N(T) - \rho_{xx}(T)}{\rho_{xx}^N(T)\rho_{xx}(T)}. \tag{2}$$

Near the onset of the transition where $\rho_{xx}(T) \ll \rho_{xx}^N(T)$, we have $\Delta\sigma_{xx}(T) \approx 1/\rho_{xx}(T)$. A common way of determining the normal-state resistivity is to use the formula proposed by

Table 2. The film thickness t_f, C-factor, coherence length $\xi_c(0)$, crossover temperature T^+, pair-breaking parameter δ and phase-relaxation time $\tau_\phi(100\ \mathrm{K})$ for the YBCO films listed in table 1.

Sample	t_f (nm)	C	$\xi_c(0)$ (Å)	T^+ (K)	δ	τ_ϕ (ps)	T^+/T_c^{mf}
1	100	10.54	1.25	96.60	0.05	0.066	1.05
2	92	3.46	2.20	100.32	0.63	0.267	1.14
3	100	1.42	2.89	104.16	2.88	0.708	1.24
4	200	31.32	1.83	94.60	0.26	0.159	1.10
5	157	5.32	1.77	88.83	0.22	0.144	1.09
6	200	3.25	2.09	92.66	0.49	0.230	1.13
7	200	5.10	1.99	92.96	0.41	0.213	1.12
8	200	16.54	1.55	87.20	0.13	0.111	1.07
9	300	4.35	2.86	70.18	2.81	0.705	1.24

Anderson and Zou [43]:

$$\rho_{xx}^N(T) = AT + B/T \tag{3}$$

where A and B are constants. This gives an excellent fit to the data, as shown in figure 3, which shows a typical plot of $\rho_{xx}T$ as a function of T^2. The curve obtained from the fit was used to extrapolate the normal-state resistivity into the fluctuation region. The parameters used in the fit, A and B, are given in table 1. Two methods are widely employed in determining the mean-field critical temperature. The first involves determining the intersection of the tangent and the inflection point of the transition curve [33]. The second method involves plotting $1/\Delta\sigma_{xx}^2$

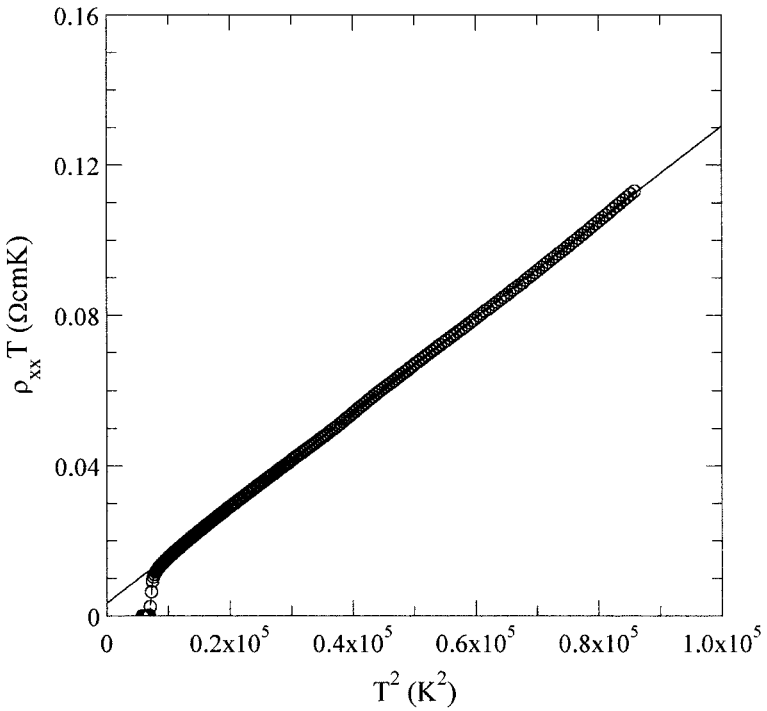

Figure 3. $\rho_{xx}T$ as a function of T^2 for sample Y116SP. The solid line is the fit to the experimental data.

against T and determining the intersection of the linear extrapolation with the T-axis which gives the mean-field critical temperature T_c^{mf} [6, 44]. This latter method was employed in this paper; see figure 4. The results for a number of films are recorded in table 1. Figure 5 shows plots of the critical temperatures against the non-stoichiometry constant x. These results are in general agreement with bulk values [45] and other published work [40, 46, 47].

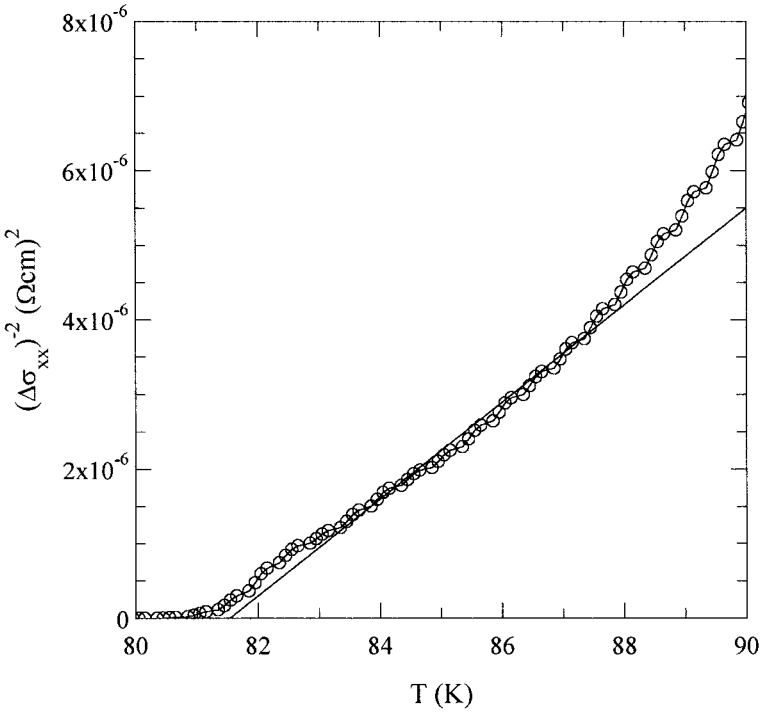

Figure 4. $\Delta\sigma_{xx}^{-2}$ as a function of temperature used to determine T_c^{mf} for sample Y84MP.

4. Discussion

The normalized resistivity ($\rho_n = \rho(T)/\rho_{300}$) versus temperature curves in figure 2 show a nearly linear temperature dependence for temperatures between 150 and 300 K. The variation of the resistivity in the a–b plane with oxygen doping has been extensively investigated [46, 48]. As x decreases below optimal doping ($x = 6.9$–7.0), corresponding to the maximum T_c, the resistivity deviates from linearity in the region 100–150 K and T_c decreases (samples 2, 3, 4, 5). Although this effect is not particularly clear in figure 3 due to normalization and the overlapping curves, careful examination shows that deviations from linearity occur at temperatures below 150 K. This is apparent for samples 2 and 3 where $x = 6.88$ and 6.78 respectively. In general the temperature behaviour of the normal-state resistivity is in good agreement with a nearly antiferromagnetic Fermi liquid (NAFL) model where at low dopings ($x = 6.45$–6.55) the resistivity curve becomes 'S' shaped as a result of the strong influence of spin fluctuations [49].

The paraconductivity was calculated from the resistivity results using equation (2) and compared with theoretical calculations based on the direct and indirect contributions to the paraconductivity. The direct contribution is due to the acceleration of superconducting quasiparticles; see Aslamasov and Larkin [1]. The indirect contribution is due to the interaction

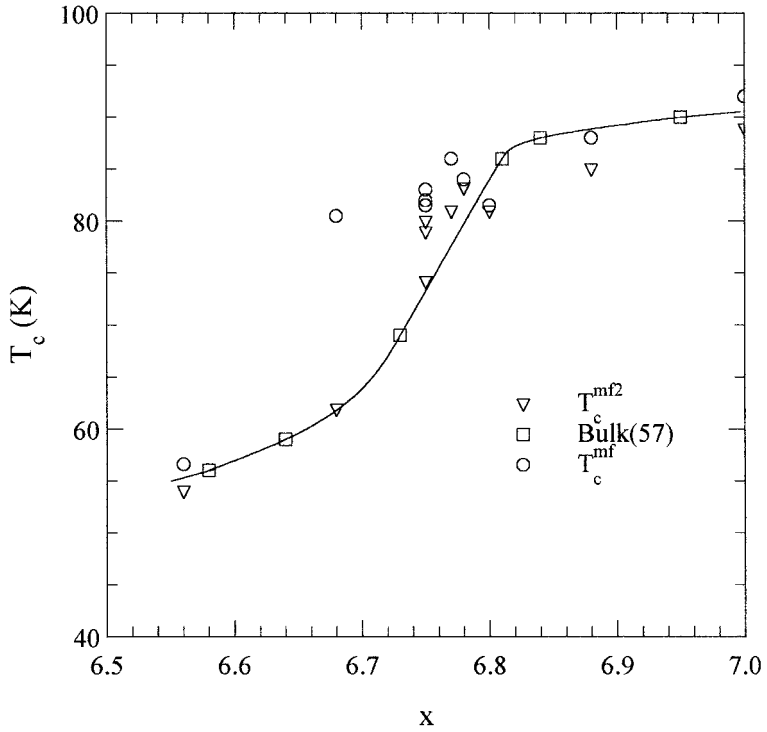

Figure 5. Mean-field critical temperatures as a function of the non-stoichiometry factor x: T_c^{mf} obtained from $\Delta\sigma_{xx}^{-2}$ versus T plots as used in this paper; T_c^{mf2} obtained from the intercept of the steepest slope of the resistivity transition. Also shown are values for bulk YBCO from reference [45].

between the superconducting pairs and the normal electrons; see Maki [2] and Thompson [3]. The Aslamasov–Larkin equations are

$$\Delta\sigma^{AL}(2\mathrm{D}) = \frac{e^2}{16\hbar\varepsilon t_f} \qquad \Delta\sigma^{AL}(3\mathrm{D}) = \frac{e^2}{32\hbar\xi(0)\varepsilon^{1/2}} \tag{4}$$

where ε, $\hbar$, t_f and $\xi(0)$ are the electron charge, reduced Planck's constant, film thickness and zero-temperature Ginzburg–Landau coherence length respectively. $\varepsilon = \ln(T/T_c^{mf}) \approx (T - T_c^{mf})/T_c^{mf}$. These expressions were extended by Lawrence and Doniach [4] to the case of layered superconductors, consisting of stacks of two-dimensional superconducting sheets linked by Josephson junctions. They obtained

$$\Delta\sigma_{xx}^{LD} = \frac{e^2/(16\hbar d)}{(1+2\alpha)^{1/2}\varepsilon} \tag{5}$$

where d is the distance between adjacent layers and α is a dimensionless coupling parameter given by

$$\alpha = 2\xi_c^2(T)/d^2 = 2\xi_c^2(0)/(d^2\varepsilon) \tag{6}$$

where $\xi_c(0)$ is the zero-temperature Ginzburg–Landau coherence length along the c-axis. The parameter α defines the crossover from the two-dimensional to the three-dimensional regime close to T_c, when the temperature-dependent coherence length along the c-axis becomes larger than d.

The FC theory for high-temperature superconductors, considering both direct and indirect contributions, has been developed by Hikami and Larkin [50]. For the indirect contribution the model gives

$$\Delta\sigma_{xx}^{MT} = \frac{e^2}{8\hbar d}\frac{1}{\varepsilon(1-\alpha/\delta)}\ln\left[\frac{\delta}{\alpha}\frac{1+\alpha+(1+2\alpha)^{1/2}}{1+\delta+(1+2\delta)^{1/2}}\right] \tag{7}$$

where

$$\delta = \frac{8\alpha k_B T\tau_\phi\varepsilon}{\pi\hbar} = \frac{16\xi_c^2(0)k_B T\tau_\phi}{\pi\hbar d^2} \tag{8}$$

is a pair-breaking parameter and τ_ϕ is the phase-relaxation time of the quasiparticles [51]. The total fluctuation conductivity is then the sum of the Lawrence–Doniach (LD) and the Maki–Thompson (MT) terms:

$$\Delta\sigma_{xx} = \Delta\sigma_{xx}^{LD} + \Delta\sigma_{xx}^{MT}. \tag{9}$$

The results of the paraconductivity calculations are recorded in table 2. In table 3 we list for comparison some literature values for YBCO thin films, single crystals and polycrystalline samples. The paraconductivity is plotted in figure 6 for several YBCO films in the reduced-temperature range (Ginzburg–Landau range) $0.01 < \varepsilon < 0.1$. Also shown are the theoretical LD, MT and sum (LD + MT) curves. The experimental data lie below the theoretical ones by a scale factor C, which is different for each sample; see table 2. In similar studies, values of C between 3 and 7 were found for thin films [6, 44] and $C = 6.8$ for a polycrystalline sample [22]. This variation in the C-factor is considered to arise from non-uniform current flow within the sample due to a number of sample-dependent effects including grain boundaries, uneven oxidation and microscopic cracks [6, 22, 44].

Table 3. Critical temperatures and paraconductivity data obtained from literature for thin films, single crystals and polycrystalline $YBa_2Cu_3O_x$.

Material	T_c (K)	$\xi_c(0)$ (Å)	τ_ϕ (ps)	Reference
Film	55	0.9		[7]
Crystal	62	4.5		[18]
Film	84.5–87.9	1.75		[6]
Film	85.5	1.5	0.10	[8]
Crystal	87–89	1.35		[14]
Film	88.55	1.5	0.086	[5]
Film	89.1	1.5		[17]
Crystal	90	1.2		[16]
Film	90.7	1.2	0.095	[10]
Crystal	92	3		[18]
Polycrystal	92	1.23		[23]
Crystal	92.3	2.3	0.100	[15]
Crystal		2.9	0.100	[20]
Film		3.2	0.080	[9]
Film		1.5	0.025	[11]
Crystal		1.5	0.140	[21]
Average		2.06	0.091	

Some of the large C-factors found here are related to the large variation in resistivity and oxygen deficiency between films. Although it is difficult to determine whether it is the oxygen deficiency or the defects that are making the main contribution, our c-axis measurements suggest that it is the former. Evidence for this is shown in figure 5 which compares our T_c-results with bulk values as a function of oxygen deficiency x.

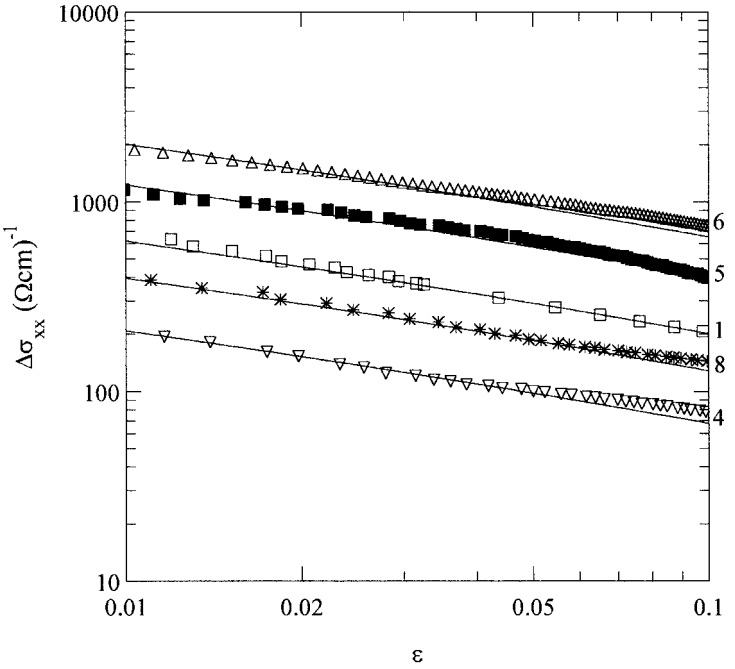

Figure 6. Typical paraconductivity results versus the reduced temperature for several YBCO films. The solid lines correspond to the ratio $(\Delta\sigma_{xx}^{LD} + \Delta\sigma_{xx}^{MT})/C$ where the C-values are listed in table 2.

The theoretical fit contains the adjustable parameters $\xi_c(0)$ in the LD term and δ in the MT term. The interlayer distance d is assumed equal to the c-axis lattice parameter. The coherence length results extracted from the fit are given in table 2. The values found are consistent with data reported in the literature for thin films, single crystals and polycrystalline samples of YBCO; see table 3 and references [52–56].

The LD model predicts a crossover from the three-dimensional to the two-dimensional behaviour at $\varepsilon^+ = (2\xi_c(0)/d)^2$ and the crossover temperature is $T^+ = T_c^{mf}(1 + \varepsilon^+)$. The results for the crossover temperature obtained from the fit between theory and data are shown in table 2. In order to determine T^+ graphically, $\Delta\sigma_{xx}$ was plotted against ε on a log–log scale; see figure 7. The comparison between theory and experiment is limited to the reduced-temperature range $0.01 < \varepsilon < 0.1$ where the theory applies. In this region, the experimental data do not show a sharp change in slope due to the change from 2D to 3D conductivity. Close to T_c^{mf}, the LD curve follows $\varepsilon^{-1/2}$ 3D behaviour, whilst at higher temperatures it follows ε^{-1} 2D behaviour. The dimensional crossover takes place at $\varepsilon = \varepsilon^+ = (2\xi_c(0)/d)^2$. On the other hand, the MT term remains finite as ε goes to zero and gives a curve with a smaller slope. In the experimental data, there is evidence for the slope changing between a half and unity as shown in figure 7, but extraction of T^+ by this method is inaccurate due to the lack of sharpness in the slope change.

The experimental results suggest an increase in $\xi_c(0)$ as c increases or as T_c decreases as shown in figure 8. In particular, there is a sharp variation in $\xi_c(0)$ at about $c = 11.71$ Å which coincides with the T_c–x transition region of the YBCO stoichiometry (figure 2). Hence, the general variation of the coherence length with lattice constant seen in figure 8 is related to the change of oxygen in the unit cell. This is expected because of the small size of the coherence length compared with the unit-cell dimensions, at least in the c-direction.

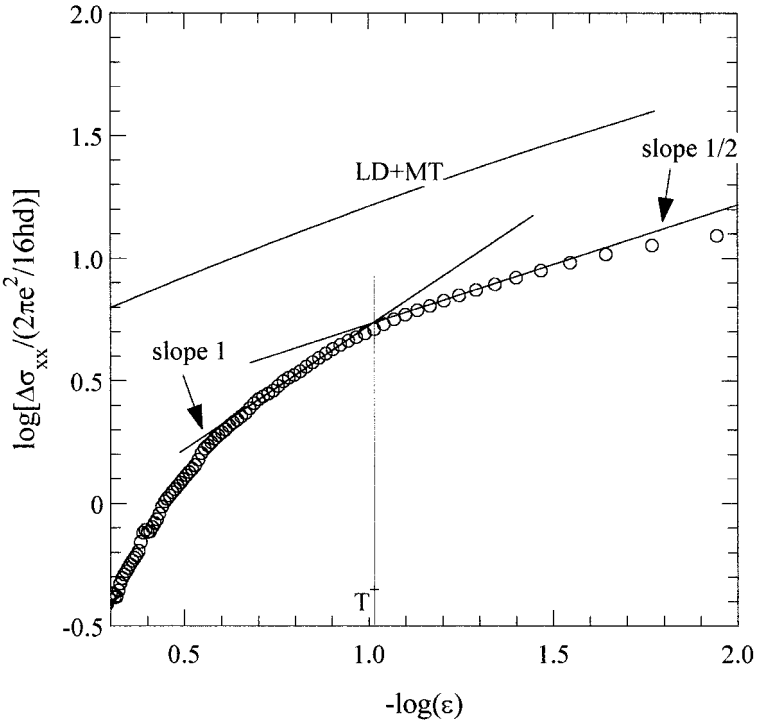

Figure 7. Theoretical and graphical extraction of the crossover temperature T^+. The theoretical value occurs when the LD slope changes from 1 to 1/2. The value determined from the measured data (circles) is imprecise due to the lack of a sharp slope change. T^+ was therefore obtained by fitting the experimental data to the models and extracting T^+ from the theory.

If the coherence length is identified with the distance Δx in the uncertainty relationship, then $\xi_c(0) \approx \hbar v_F/(k_B T_c)$ where v_F is the velocity of the carriers at the Fermi level [57]. The Fermi velocity would therefore need to be constant, or at least change by a small amount compared with the change of T_c, in order to obtain agreement with the experimental results. A measure of v_F may be obtained from the electron mobility where $\xi_c(0) \approx \mu E_x \hbar/(k_B T_c)$ where μ is the mobility and E_x is the longitudinal electric field. For our oxygen-deficient samples, it is known that the Hall mobility is higher for the higher-T_c samples [32]. However, it is questionable whether these results are applicable here, since normal-state effects are minimized by subtracting the normal-state conductivity.

The phase-relaxation time may be determined from equation (8):

$$\tau_\phi = \frac{\pi \hbar d^2 \delta}{16 \xi_c^2(0) k_B T}. \tag{10}$$

Figure 9 shows a plot of τ_ϕ against T_c^{mf} using data from table 2. This indicates a general decrease in τ_ϕ with increasing critical temperature. We note that, at a constant temperature ($T =$ 100 K), $\delta \propto 1/T_c^{mf}$ (table 2) and $\xi_c(0) \propto d$ or c (figure 8). Thus $\tau_\phi \propto d^2/(d^2 T_c^{mf}) = 1/T_c^{mf}$. Hence, we expect the phase-relaxation time to decrease with increasing critical temperature.

We can also compare this more directly with the uncertainty relation, $\Delta E\, \Delta t \geqslant \hbar/2$. Assuming that $\Delta t = \tau_\phi$ and $\Delta E = \alpha k_B T_c$, we have $\tau_\phi = \hbar/(2\alpha k_B T_c)$ which again suggests that τ_ϕ decreases with increasing T_c.

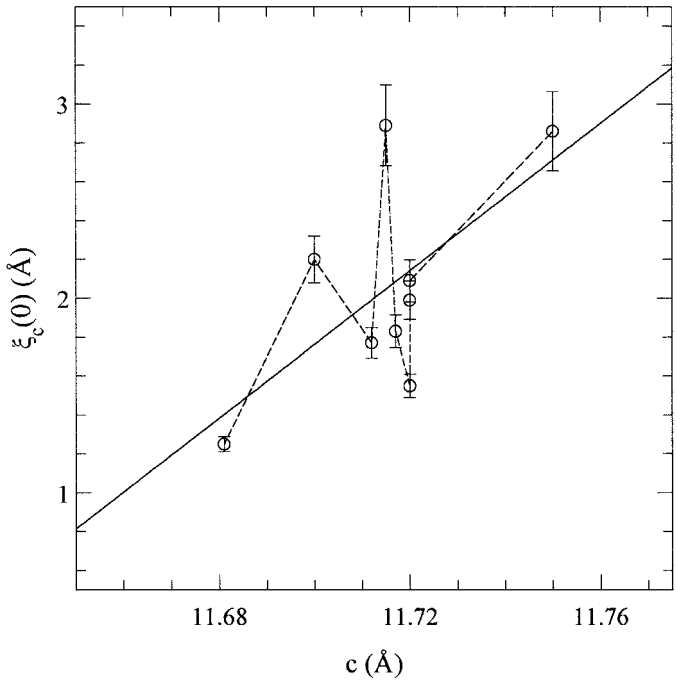

Figure 8. The coherence length $\xi_c(0)$ against the YBCO c-axis lattice parameter. The solid line is a least-squares fit to the data.

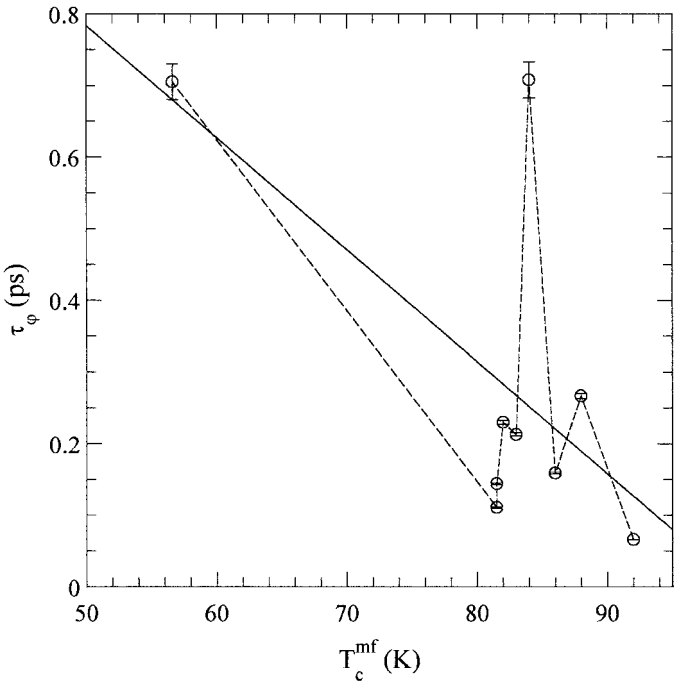

Figure 9. Phase-relaxation time $\tau_\phi(100\,\mathrm{K})$ as a function of the mean-field critical temperature T_c^{mf} for various YBCO films. The solid line has a gradient of -0.015 ps K^{-1}.

It is of interest to compare the measured relaxation time $\tau_\mu = m^*\mu(T)/q$ with the phase-relaxation time τ_ϕ. Taking $m^* = 5m_0$, we have $\tau_\mu = 2.843\,\mu(T)$ ps [32]. At 100 K, $\mu = 20 \times 10^{-4}$ m^2 V^{-1} s^{-1} for samples with $T_c = 85$ K, giving $\tau_\mu = 5.686 \times 10^{-15}$ s. Also at 100 K, $\mu = 1 \times 10^{-4}$ m^2 V^{-1} s^{-1} for samples with $T_c = 54$ K, giving $\tau_\mu = 2.843 \times 10^{-16}$ s. These values are small compared with τ_ϕ, which varies between 0.1 and 0.7 ps at 100 K. For the samples analysed, we find that the ratio τ_ϕ/τ_μ decreases with increasing oxygen content x, giving $\tau_\phi/\tau_\mu = 47$ for $x = 6.9$ and $\tau_\phi/\tau_\mu = 2480$ for $x = 6.56$. However, in the region near the T_c–x (60 K) transition (figure 5), τ_ϕ varies sharply.

Although, in general, we find that our values of the coherence length and phase-relaxation time are in good agreement with other published work, specific details vary. Previous results have indicated that $\xi_c(0)$ increases with oxygen content x [46], but we find that $\xi_c(0)$ varies in a complex way near the 60 K transition in the T_c–x phase diagram (see figure 10) and is probably related to the formation of the O II superlattice [47].

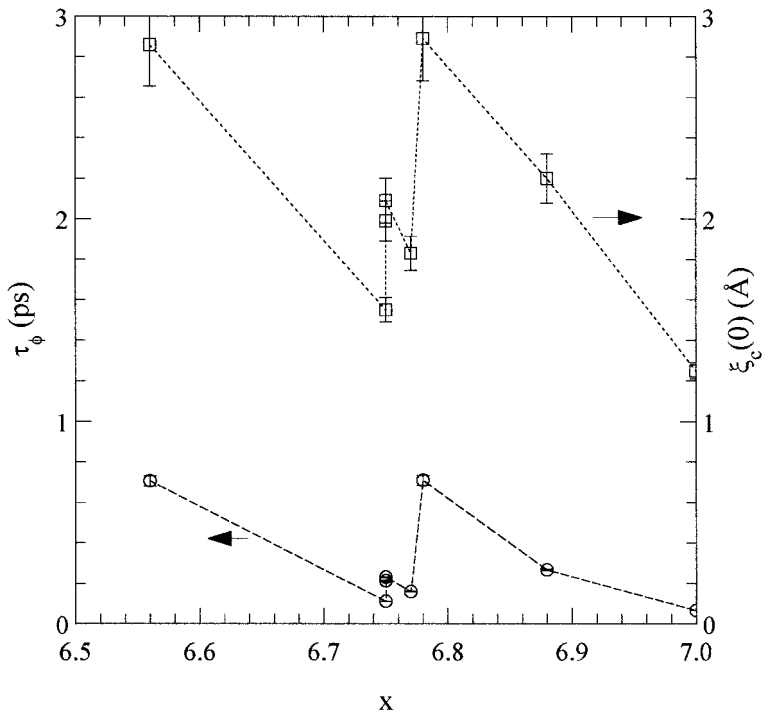

Figure 10. Coherence length and phase-relaxation time as functions of the non-stoichiometry factor x. The transitions occur close to the 60 K transition in the T_c–x diagram.

Our results were obtained for a number of films prepared using an *in situ* oxidation process, whereas the results of reference [46] were obtained from a single film using an *ex situ* oxidation treatment. In our *in situ* process the final oxidation takes place immediately after growth as the film cools in the surrounding oxygen gas; during this process, the film structure changes from tetragonal to orthorhombic. The *ex situ* process involves taking a fully oxygenated film, after growth, and converting it to the required stoichiometry by heating in oxygen. This suggests that the two oxidation processes may lead to different sets of lattice defects in these non-stoichiometric compounds—a conclusion which was arrived at from previous mobility measurements [32].

5. Summary

We have presented measurements of the resistivity of r.f.-sputtered *c*-axis-oriented $YBa_2Cu_3O_x$ thin films as a function of temperature. The Anderson and Zou [43] formula was used to extrapolate the normal-state resistivity into the fluctuation region. Paraconductivity data were obtained first by fitting the measured data to the sum of LD and MT fluctuation theories using a fitting parameter, C. The results obtained for optimally doped films are in general agreement with other work. There was considerable scatter in the coherence length and phase-relaxation time for films with different critical temperatures and oxygen contents. These results were process dependent but appear to be related to the 60 K phase transition in the T_c–x phase diagram and are probably related to the formation of the O II superlattice [47].

Acknowledgments

The authors wish to thank the Algerian Ministry for Higher Education (MESRS) and the British Council for providing grants to A Gueffaf, and the Syrian Government and the University of Damascus for supporting M Salim.

References

[1] Aslamasov L G and Larkin A I 1968 *Fiz. Tverd. Tela* **10** 1104 (Engl. Transl. 1968 *Sov. Phys.–Solid State* **10** 875)
[2] Maki K 1968 *Prog. Theor. Phys.* **39** 897
[3] Thompson R S 1970 *Phys. Rev.* B **1** 327
[4] Lawrence W E and Doniach S 1971 *Proc. 12th Int. Conf. on Low Temperature Physics (Kyoto, 1970)* ed E Kanda (Tokyo: Keigaku) p 361
[5] Lang W, Heine G, Schwab P, Wang X Z and Bäuerle D 1994 *Phys. Rev.* B **49** 4209
[6] Oh B, Char K, Kent A D, Naito M, Beasley M R, Geballe T H, Hammond R H, Kapitulnik A and Graybeal J M 1988 *Phys. Rev.* B **37** 7861
[7] Lang W, Gob W, Kula W and Sobolewski R 1995 *Z. Phys.* B **98** 453
[8] Matsuda Y, Hirai T, Komiyama S, Terashima T, Bando Y, Iijima K, Yamamoto K and Hirata K 1989 *Phys. Rev.* B **40** 5176
[9] Sugawara J, Iwasaki H, Kobayashi N, Yamane H and Hirai T 1992 *Phys. Rev.* B **46** 14 818
[10] Sekirnjak C, Lang W, Proyer S and Schwab P 1995 *Physica* C **243** 60
[11] Holm W, Rapp Ö, Johnson C N L and Helmersson U 1995 *Phys. Rev.* B **52** 3748
[12] Wang L M, Yang H C and Horng H C 1999 *Phys. Rev.* B **59** 14 031
[13] Liu W, Clinton T W, Smith A W and Lobb C J 1997 *Phys. Rev.* B **55** 11 802
[14] Hagen S J, Wang Z Z and Ong N P 1988 *Phys. Rev.* B **38** 7137
[15] Overend N and Howson M A 1992 *J. Phys.: Condens. Matter* **4** 9615
[16] Torrón C, Díaz A, Pomar A, Veira J A and Vidal F 1994 *Phys. Rev.* B **49** 13 143
[17] Gasparov V A 1991 *Physica* C **178** 449
[18] Vandervoort K G, Welp U, Kessler J E, Glaus H, Crabtree G W, Kwok W K, Umezawa A, Veal B W, Downey J W and Paulikas A P 1991 *Phys. Rev.* B **43** 13 042
[19] Iye Y 1987 *Japan. J. Appl. Phys.* **26** 4057
[20] Hikita M and Suzuki M 1990 *Phys. Rev.* B **41** 834
[21] Winzer K and Kumm G 1991 *Z. Phys.* B **82** 317
[22] Matsuda Y, Hirai T and Komiyama S 1988 *Solid State Commun.* **68** 103
[23] Lee W C, Klemm R A and Johnston D C 1989 *Phys. Rev. Lett.* **63** 1012
[24] Lang W, Heine G, Kula W and Sobolewski R 1995 *Phys. Rev.* B **51** 9180
[25] Lang W 1995 *Z. Phys.* B **97** 523
[26] Dhard C P, Bhatia S N, Sastry P V P S S, Yakhmi J V and Nigam A K 1994 *J. Appl. Phys.* **76** 6944
[27] Fu C M, Boon W, Wang Y S, Moshchalkov V V and Bruynseraede Y 1992 *Physica* C **200** 17
[28] Suzuki M and Hikita M 1991 *Phys. Rev.* B **44** 249
[29] Gonzalez M A, Prieto P, Oyola D and Vicent J L 1991 *Physica* C **185** 1287
[30] Han S H, Zhao Y, Gu G D, Russell G J and Koshizuka N 1997 *Phys. Status Solidi* b **203** 189

[31] Wang L M, Yang H C and Horng H E 1999 *Phys. Rev.* B **59** 14 031
[32] Raven M S and Wan Y M 1995 *Phys. Rev.* B **51** 561
[33] Freitas P P, Tsuei C C and Plaskett T S 1987 *Phys. Rev.* B **36** 833
[34] Ausloos M and Laurent C 1988 *Phys. Rev.* B **37** 611
[35] Hopfengärtner R, Hensel B and Saemann-Ischenko G 1991 *Phys. Rev.* B **44** 741
[36] Weigang G and Winzer K 1989 *Z. Phys.* B **77** 11
[37] Friedmann T A, Rice J P, Giapintzakis J and Ginsberg D M 1989 *Phys. Rev.* B **39** 4258
[38] Ghosh A K, Bandyopadhyay S K, Barat P, Sen P and Basu A N 1997 *Solid State Commun.* **104** 211
[39] Raven M S 1994 *J. Mater. Sci.: Mater. Electron.* **5** 129
[40] Raven M S, Inameti E E, Wan W M and Murray B G 1994 *Supercond. Sci. Technol.* **7** 462
[41] Hilton G C, Harris E B and Van Harlingen D J 1988 *Appl. Phys. Lett.* **53** 1107
[42] Ohkubo M, Kachi T, Hioki T and Kawamoto J 1989 *Appl. Phys. Lett.* **55** 899
[43] Anderson P W and Zou Z 1988 *Phys. Rev. Lett.* **60** 132
[44] Beasley M R 1987 *Physica* B **148** 191
[45] Cava R J, Hewat A W, Hewat E A, Batlogg B, Marezio M, Rabe K M, Krajewski J J, Peck W F Jr and Rupp L W Jr 1990 *Physica* C **165** 419
[46] Carrington A, Walker D J C, Mackenzie A P and Cooper J R 1993 *Phys. Rev.* B **48** 13 051
[47] Raveau B, Michel C, Hervieu M, Provost J and Studer F 1990 *Superconductivity* ed J G Bednorz and K A Müller (Berlin: Springer) p 66
[48] Iye Y 1992 *Physical Properties of High Temperature Superconductors III* ed D M Ginsberg (Singapore: World Scientific) p 285
[49] Stojković B P and Pines D 1997 *Phys. Rev.* B **55** 8576
[50] Hikami S and Larkin A I 1988 *Mod. Phys. Lett.* B **2** 693
[51] Patton B R 1971 *Phys. Rev. Lett.* **27** 1273
[52] Axnäs J, Lundqvist B and Rapp Ö 1998 *Phys. Rev.* B **58**, 6628
[53] Volz W, Rasavi F S, Quirion G, Habermeier H-U and Solovjov A L 1997 *Phys. Rev.* B **55** 6631
[54] Solovjov A L, Dmitriev V M, Habermeier H-U and Trofimov I E 1997 *Phys. Rev.* B **55** 8551
[55] Bieri J B and Maki K 1990 *Phys. Rev.* B **42** 4854
[56] Bieri J B, Maki K and Thompson R S 1991 *Phys. Rev.* B **44** 4709
[57] Burns G 1992 *High-Temperature Superconductivity* (London: Academic) p 17